

Iterative Correlation-based Feature Refinement for Few-shot Counting

Zhiyuan You¹, Kai Yang², Wenhan Luo³, Xin Lu², Lei Cui², Xinyi Le^{*1}

¹Shanghai Jiao Tong University ²Sensetime ³Tencent

*Corresponding Author, xinyile@sjtu.edu.cn

Abstract

Few-shot counting aims to count objects of any class in an image given only a few exemplars of the same class. Existing correlation-based few-shot counting approaches suffer from the coarseness and low semantic level of the correlation. To solve these problems, we propose an iterative framework to progressively refine the exemplar-related features based on the correlation between the image and exemplars. Then the density map is predicted from the final refined feature map. The iterative framework includes a Correlation Distillation module and a Feature Refinement module. During the iterations, the exemplar-related features are gradually refined, while the exemplar-unrelated features are suppressed, benefiting few-shot counting where the exemplar-related features are more important. Our approach surpasses all baselines significantly on few-shot counting benchmark FSC-147. Surprisingly, though designed for general class-agnostic counting, our approach still achieves state-of-the-art performance on car counting benchmarks CARPK and PUCPR+, and crowd counting benchmarks UCSD and Mall. We also achieve competitive performance on crowd counting benchmark ShanghaiTech. The code will be released soon.

1. Introduction

Most existing visual counting methods focus on a specific class at a time, such as people [24, 36, 52, 53], animals [1], and cars [5, 12], while class-agnostic few-shot counting (FSC) counts for any class. As shown in Fig. 1(a), given an image from a novel class and a few labeled exemplars, FSC aims to count objects of the same class as the exemplars, which is a more general and challenging task.

In FSC [28], there are base classes in which both a few labeled exemplars and the locations of all objects are available and novel classes in which only a few labeled exemplars are available. The novel classes share no common classes with the base classes. FSC is expected to learn from base classes and be able to count objects of novel classes with only a few labeled exemplars. To achieve this, recent

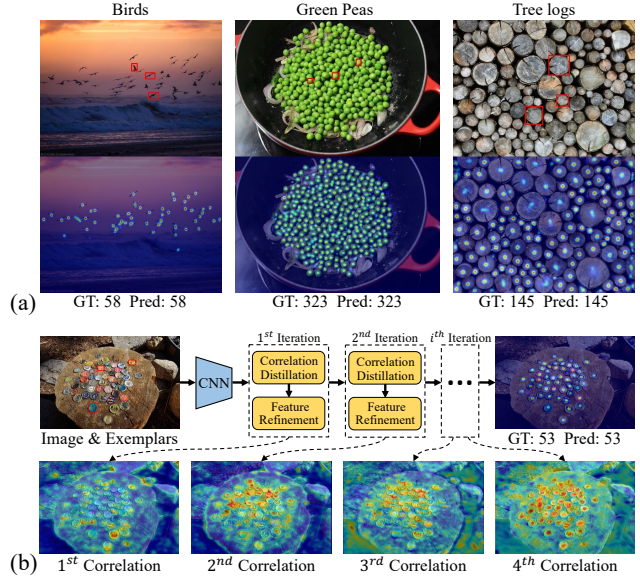


Figure 1. (a) Few-shot counting results on FSC-147 [28]. From top to down: images and the predicted density maps. The objects marked by the red rectangles are the exemplars. (b) The pipeline of our approach. The Correlation Distillation module calculates and normalizes the correlation between the image and exemplars. The Feature Refinement module refines exemplar-related features based on the normalized correlation. Both the exemplar-related features and the correlation are gradually refined with the iterations. The density map is predicted using the refined feature map.

FSC methods [25, 28] utilize the intuition that the regions more similar to exemplars are more likely to be target objects. These methods firstly calculate the correlation between the image and exemplars, then utilize the correlation to regress the density map, from which the predicted count is obtained by summing all values of the density map. However, there are two main issues about these approaches.

One issue is the **coarseness** of the correlation. It is shown in Fig. 1(b) that the correlation between the original image feature map and exemplar feature maps (denoted as 1st Correlation) is quite coarse, thus it is difficult to regress a high-quality density map from this coarse correlation. The

coarseness of the correlation is mainly caused by the disturbance of exemplar-unrelated features, such as the features of stones, trucks, and earth in this image.

Another issue is the **low semantic level** of the correlation. The correlation is just a rough estimate of the similarity between the input image and exemplars, and the semantic information in the correlation is quite poor. In contrast, the CNN-extracted features contain rich semantic information that is beneficial for density regression. However, regressing the density map directly from the feature map suffers from the fact that there are too many disturbing exemplar-unrelated features.

In this paper, considering the vital significance of the exemplar-related features in FSC, we propose an iterative correlation-based feature refinement framework to progressively refine the exemplar-related features and suppress the exemplar-unrelated features. As illustrated in Fig. 1(b), from the 1st to 4th iteration, there are less and less disturbance of the exemplar-unrelated features and the correlation is also iteratively refined. More importantly, since the exemplar-unrelated features have been suppressed, we could regress the density map directly from the semantic-rich refined feature map instead of the semantic-poor correlation. Therefore, our approach solves the above two main issues and achieves state-of-the-art FSC performance, as the FSC results in Fig. 1(a) demonstrate.

The proposed framework is composed of the Correlation Distillation module and the Feature Refinement module as shown in Fig. 1(b). The Correlation Distillation module is used to calculate and normalize the correlation between the image and exemplars. The Feature Refinement module refines the feature map based on the normalized correlation. By doing so, the exemplar-related features, *i.e.* the features of the regions more similar to the exemplars, would correspond to higher correlation values. These exemplar-related features would also be better refined, boosting the FSC performance which relies more highly on exemplar-related features. We summarize our contributions as follows:

- We propose an iterative FSC framework including a Correlation Distillation module and a Feature Refinement module to iteratively refine the exemplar-related features. The refinement framework allows us to regress the density map directly from the semantic-rich feature map instead of the semantic-poor correlation.
- We propose a Correlation Distillation module to calculate and normalize the correlation between the image and exemplars, obtaining a normalized correlation with proper scales for better feature refinement.
- We propose a Feature Refinement module to refine exemplar-related features using the normalized correlation, promoting the performance of FSC in which exemplar-related features are more important.
- Extensive experiments conducted on FSC benchmark FSC-147 [28], car counting benchmarks CARPK [12] and PUCPR+ [5, 12], and crowd counting benchmarks UCSD [3], Mall [4], and ShanghaiTech [53] demonstrate that our approach achieves state-of-the-art counting performance.

2. Related Work

Object counting approaches could be roughly divided into class-agnostic ones and class-specific ones.

Class-agnostic counting approaches aim to count objects of different classes. IEP Counting [37] divides images into several regions, then regresses the count by inclusion-exclusion principle. PDEM [9] proposes Soft-IoU and EM-Merger, helping object detection and counting in densely packed scenes. In [17], a localization-based counting loss is proposed, formulating counting as a segmentation problem. However, [9, 17, 37] could only work on close-set benchmarks where the classes in the test set are the same as those in the training set, which does not fulfill the requirements of FSC. GMN [25] and FamNet [28] both utilize the correlation to regress the density map for FSC. However, after pre-trained on ILSVRC dataset [31], GMN still needs to be re-trained with dozens or hundreds of annotated images for adaption when used for new classes. Also, the coarseness and low semantic level of correlation decrease the performance of GMN and FamNet, as described in Sec. 1.

Class-specific counting approaches count objects of a specific class at a time, such as people [24, 36, 52, 53], animals [1], cars [5, 12], among which crowd counting has been widely researched. For crowd counting, traditional methods [18, 38, 43] count the crowd number in an image by detecting persons, which does not work well for images with high crowd density. Recent methods mainly use a deep neural network to predict the density map [42] from the crowd image, where the sum over the density map is the crowd count [19]. Various crowd counting approaches have been proposed to handle perspective distortion [47, 49], to address scale variation [2, 53], to refine the predicted density map [27, 32, 33], and to encode context information [34, 46], continuously improving the crowd counting performance. A cross-scene crowd counting method is proposed in [50] to improve the generalization ability. [23] uses a detector and a regressor to estimate the crowd count and proposes a Decidet to merge the two predicted results. Recently, [36, 41] propose novel loss functions that predict quite accurate position of each person, highly improving the crowd localization ability. For animal counting, [1] augments density estimation with foreground-background segmentation and explicit local uncertainty estimation to count penguins. For car counting, [12] proposes LPNs with spatial kernels to simultaneously count and localize cars. However, these methods could count objects of only one specific class at a time.

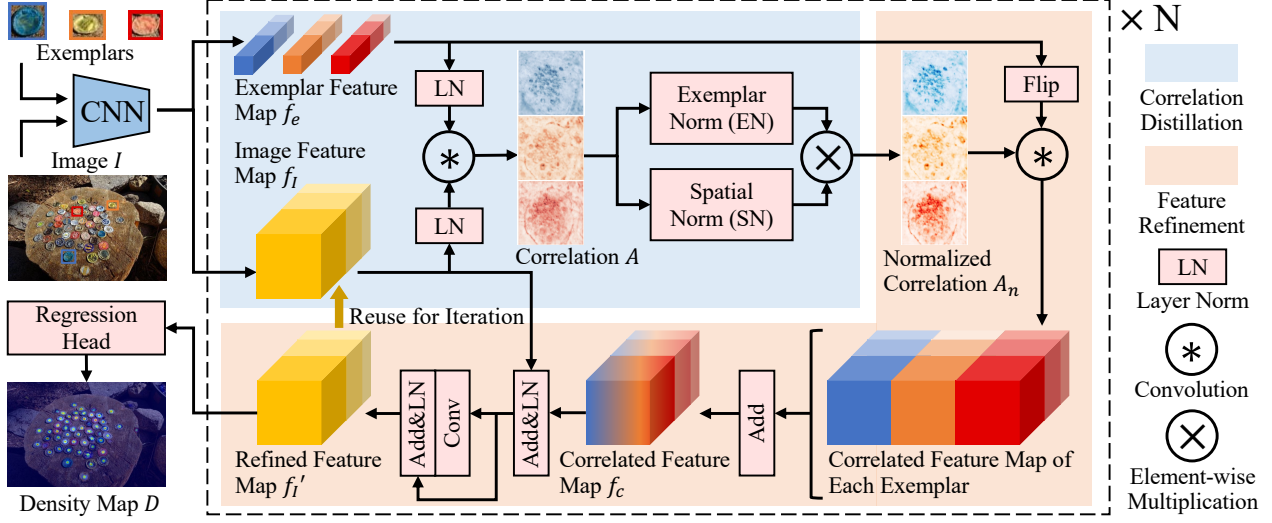


Figure 2. **The framework of our approach.** Firstly, a frozen pre-trained CNN backbone is adopted for feature extraction. Then, the Correlation Distillation module calculates and normalizes the correlation between the image feature map and the exemplar feature map. Afterwards, the Feature Refinement module calculates the correlated feature map based on the normalized correlation. The correlated feature map and the input image feature map are fused to obtain the refined feature map, which could be reused for the next iteration. After N iterations, the density map is regressed using the final refined feature map.

Few-shot approaches are also highly related with our work. Few-shot classification [8, 44], detection [6, 45], and segmentation [48, 51] aim to complete corresponding tasks on images of novel classes given a few exemplars. For classification, MAML [8] learns parameters which can adapt to novel classes at test time by few gradient descent steps. FRN [44] formulates few-shot classification as a reconstruction problem in latent space. For detection, [6] exploits the similarity between the input image and the exemplars to detect novel objects while suppressing false detection in the background. [45] generates multi-scale positive samples as object pyramids and refines the prediction at various scales. For segmentation, [51] proposes a two-branch dense comparison module performing multi-level feature comparison between the input image and the exemplars, and the segmentation results are iteratively refined. [48] aims to alleviate the problem of feature undermining and enhance the feature embedding of latent novel classes. However, researches for few-shot counting are still limited.

3. Method

In this section, we first briefly introduce the preliminaries for few-shot counting (FSC) in Sec. 3.1. Then the proposed iterative feature refinement framework is described in Sec. 3.2, following the detailed architectures of the Correlation Distillation module and the Feature Refinement module in Sec. 3.3. Finally, we provide a theoretical comparison between our method and the transformer in Sec. 3.4. The overall framework of our approach is shown in Fig. 2.

3.1. Few-shot Counting Preliminaries

In FSC [28], object classes are divided into base classes C_b and novel classes C_n , where C_b and C_n have no intersection. For each image from C_b , both a few corresponding exemplars and the locations of all target objects are provided. While, for the images from C_n , only their corresponding exemplars are available. FSC aims to count target objects from C_n with only a few annotated exemplars by leveraging the generalization knowledge from C_b . Denote the number of exemplars per image as K , the task is called K -shot FSC.

3.2. Iterative Feature Refinement Framework

Given an image $I \in \mathbb{R}^{C_I \times H_I \times W_I}$, a frozen ImageNet pre-trained ResNet-18 [11] is applied to extract features. The feature maps from layer1 to layer3 are selected. These feature maps are firstly resized to the same size $H \times W$, then concatenated together to form a multi-layer image feature map $f_I \in \mathbb{R}^{C \times H \times W}$. The feature maps of the exemplars are calculated by ROI Pooling [30] on the corresponding multi-layer image feature map. Then the feature maps of all exemplars are concatenated together to obtain the exemplar feature map $f_e \in \mathbb{R}^{K \times C \times H_e \times W_e}$, where K is the number of exemplars, H_e, W_e are manually selected size.

In the **Correlation Distillation** module, the correlation A between the image feature map f_I and the exemplar feature map f_e is firstly calculated. Then we propose exemplar normalization (EN) and spatial normalization (SN) to respectively normalize the correlation A among different exemplars and spatial positions, providing a normalized cor-

relation A_n with proper scales for better feature refinement. The **Feature Refinement** module firstly calculates the correlated feature map f_c based on the normalized correlation A_n . Here the name ‘‘correlated feature map’’ means that the features in this feature map are highly related to the normalized correlation A_n . Specifically, the features corresponding to larger correlation values are better retained. Then this module fuses the correlated feature map f_c with the input image feature map f_I to obtain the refined feature map f'_I . In essence, the feature refinement is instructed by the normalized correlation A_n . The features of the positions whose correlation values are large, *i.e.* the exemplar-related features, would be better refined. This boosts the performance of FSC in which the exemplar-related features are more crucial. The Correlation Distillation module and the Feature Refinement module are detailed in Sec. 3.3.

The refined feature map f'_I could serve as the inputs to the next iteration. The N iterations would progressively refine the exemplar-related features and suppress the exemplar-unrelated features. Without the disturbance of the exemplar-unrelated features, we could regress the density map $D \in \mathbb{R}^{H_I \times W_I}$ directly from the semantic-rich refined feature map instead of the semantic-poor correlation. The regression head is composed of iterative convolution, ReLU activation, and bi-linear up-sample. Its detailed architecture is given in the Supplementary Material.

The annotations of most counting datasets are dots, indicating the object positions. However, it is difficult to train a network with the dot annotations directly. Most existing methods generate ground truth (GT) density maps for training. Following [28], we utilize the Gaussian smoothing with adaptive window size to generate the GT density maps. The GT density map for image I is denoted as $D_{gt} \in \mathbb{R}^{H_I \times W_I}$. Our model is trained with MSE loss \mathcal{L} as follows,

$$\mathcal{L} = \text{MSE}(D - D_{gt}). \quad (1)$$

The training configuration is detailed in Sec. 4.

3.3. Module Architecture

Correlation Distillation module is used to calculate and normalize the correlation between the image feature map and the exemplar feature map. In [28], the correlation A is obtained by directly convoluting the image feature map f_I with the exemplar feature map f_e as the convolution kernel. However, we found that this implementation is unstable and easy to diverge during training. We suspect the reason might be that the scales of feature maps vary largely for different images and objects. Layer normalization (LN) normalizes the feature maps of different images and objects to ensure the same distribution and similar scales. Thus the instability problem could be resolved by adding a shared LN layer before the convolution between f_I and f_e as follows,

$$A = \text{LN}(f_I) * \text{LN}(f_e) \in \mathbb{R}^{K \times H \times W}. \quad (2)$$

The scales of correlation values should be normalized to better refine features, for which we propose Exemplar Normalization (EN) and Spatial Normalization (SN). EN aims to seek the normalization among different exemplars, which is a softmax layer as follows,

$$A_e = \text{softmax}\left(\frac{A}{\sqrt{H_e W_e C}}, \dim = 0\right) \in \mathbb{R}^{K \times H \times W}, \quad (3)$$

where $\text{softmax}(\cdot, \dim)$ is the softmax layer operated on a specific dimension. However, EN ignores the spatial difference. With only EN, the sum of correlation values of different exemplars in a specific position is 1, which means that the sum of correlation values of a high-relevant position equals that of a low-relevant position. This problem is solved by the introduction of SN. SN is used to normalize among different spatial positions. After SN, the correlation value of the most relevant position would be 1, and others would be among $[0, 1]$. The formula is

$$\begin{aligned} A' &= \exp\left(\frac{A}{\sqrt{H_e W_e C}}\right) \in \mathbb{R}^{K \times H \times W}, \\ A_s &= \frac{A'}{\max(A', \dim = (1, 2))} \in \mathbb{R}^{K \times H \times W}, \end{aligned} \quad (4)$$

where $\max(\cdot, \dim)$ is used to find the maximum value among specific dimensions. Finally, the exemplar normalized correlation A_e and the spatial normalized correlation A_s are fused by the element-wise multiplication to obtain the final normalized correlation $A_n \in \mathbb{R}^{K \times H \times W}$ as,

$$A_n = A_e \otimes A_s. \quad (5)$$

The ablation study of normalization in Sec. 4.5 indicates that both EN and SN improve the performance significantly.

Feature Refinement module firstly calculates the correlated feature map based on the normalized correlation, then obtains the refined feature map by feature fusion. In our design, the correlated feature map should be highly related to the normalized correlation. Namely, the larger the correlation value of a specific position is, the more related to exemplars its corresponding feature is, the better this feature should be maintained. Therefore, the values of the normalized correlation A_n are viewed as the weights of combining the exemplar feature map f_e to acquire the correlated feature map f_c . The combination process is illustrated as follows. First, the exemplar feature map f_e is flipped horizontally and vertically. Then, we convolute the normalized correlation A_n with the flipped exemplar feature map as the convolution kernel to obtain the correlated feature map f_c . Here the convolution is done independently with each exemplar, then the results are summed to acquire the correlated feature map f_c . The formula is

$$\begin{aligned} f' &= A_n * \text{flip}(f_e) \in \mathbb{R}^{K \times C \times H \times W}, \\ f_c &= \text{sum}(f', \dim = 0) \in \mathbb{R}^{C \times H \times W}, \end{aligned} \quad (6)$$

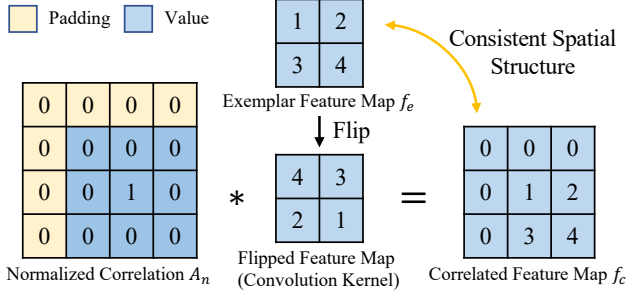


Figure 3. **Calculation of the correlated feature map.** The flip helps the correlated feature map keep consistent spatial structure as the exemplar feature map.

where $\text{sum}(\cdot, \text{dim})$ is the sum among specific dimensions. Besides, the reason why we add flip is shown in Fig. 3. The flip helps the correlated feature map retain consistent spatial structure as the exemplar feature map, whose advantages are verified in the ablation study in Sec. 4.5.

The correlated feature map f_c is fused with the input image feature map f_I to obtain the refined feature map f'_I by shortcut connection, convolution and LN, as shown in Fig. 2. The refined feature map f'_I could serve as the inputs to the next iteration for further feature refinement. The iterative refinement framework gradually refines the exemplar-related features, promoting the performance of FSC where the exemplar-related features are more significant.

3.4. Comparison with Transformer

Essentially, our method is closely related to the self-attention module in transformer [39], which is defined as,

$$\text{Attention}(\mathbf{q}, \mathbf{k}, \mathbf{v}) = \text{softmax}\left(\frac{\mathbf{q} \cdot \mathbf{k}}{\sqrt{d_k}}\right)\mathbf{v}, \quad (7)$$

where $\mathbf{q}, \mathbf{k}, \mathbf{v}$ are respectively the query, key, and value, d_k is the channel number of tokens. The dot multiplication between \mathbf{q} and \mathbf{k} can be taken as correlation calculation. The division by $\sqrt{d_k}$ and the softmax can be seen as correlation normalization. The multiplication with \mathbf{v} can be seen as calculating the correlated feature map with normalized correlation. Also, transformer has shortcut connections and feed-forward networks for feature fusion. The difference lays in that our method is based on convolution and keeps the spatial structure of feature maps, while transformer splits feature maps into independent tokens resulting in the loss of spatial structure. The ablation study in Sec. 4.5 shows that keeping the spatial structure brings a large improvement.

4. Experiments

4.1. Evaluation Metrics

We choose Mean Absolute Error (MAE) and Root Mean Squared Error (RMSE) to measure the performance of ob-

ject counting approaches following [9, 24, 28]:

$$MAE = \frac{1}{N_I} \sum_{i=1}^{N_I} |C_i - C_i^{GT}|, \quad (8)$$

$$RMSE = \sqrt{\frac{1}{N_I} \sum_{i=1}^{N_I} (C_i - C_i^{GT})^2}, \quad (9)$$

where N_I is the number of images, C_i and C_i^{GT} are the predicted and ground truth count of the i^{th} image, respectively.

4.2. Datasets

FSC-147 [28] is a multi-class FSC dataset with 147 classes and 6135 images. The number of objects per image varies extremely from 7 to 3701 with an average of 56. Each image has 3 exemplars for counting. It is worth noting that FSC-147 is an open-set counting benchmark. The training set contains 89 classes, while the validation set and test set both contain another disjoint 29 classes. In addition, the images collected from COCO [22] dataset in the validation set and test set of FSC-147 are named as Val-COCO and Test-COCO, which comprise of 277 and 282 images, respectively. These two COCO subsets are also used as an FSC evaluation benchmark, especially for the comparison with detection-based approaches considering that COCO is a widely adopted object detection benchmark.

Car counting datasets. **CARPK** [12] is a car counting dataset with 1448 images and nearly 90,000 cars from a drone perspective. These images are collected in various scenes of 4 different parking lots. The training set contains 3 scenes, while another scene is used for testing. **PUCPR+** [5, 12] is a camera-shot car counting dataset with 125 images and nearly 17,000 cars. The number of cars per image varies extremely from 0 to 331. The training set contains 100 images and the rests are used for test.

Crowd counting datasets. **ShanghaiTech** [53] contains 1198 annotated images with 330,165 persons in total. This dataset consists of two parts as PartA containing 482 images with highly congested scenes downloaded from the Internet and PartB including 716 images with relatively sparse crowd scenes taken from streets in Shanghai. **UCSD** [3] is a dataset of 2000 frames captured by surveillance cameras. These scenes contain sparse crowds varying from 11 to 46 persons per image. **Mall** [4] contains over 60,000 pedestrians in 2000 video sequences taken in a mall. For both UCSD and Mall, 800 frames are employed for training and the remaining 1200 frames are used for testing.

4.3. Class-agnostic Few-shot Counting

The class-agnostic FSC performance of our approach is evaluated on the FSC-147 [28] dataset.

Setup. The sizes of the image, the multi-layer feature map, and the exemplar feature map are selected as

Table 1. **The few-shot counting performance on FSC-147.** We significantly surpass all baseline approaches by a large margin.

Method	Val Set		Test Set	
	MAE ↓	RMSE ↓	MAE ↓	RMSE ↓
FR few-shot detector [13]	45.45	112.53	41.64	141.04
FSOD few-shot detector [7]	36.36	115.00	32.53	140.65
Pre-trained GMN [25]	60.56	137.78	62.69	159.67
GMN [25]	29.66	89.81	26.52	124.57
MAML [8]	25.54	79.44	24.90	112.68
FamNet [28]	23.75	69.07	22.08	99.54
Ours	15.28	47.20	14.32	85.54

Table 2. **The few-shot counting performance on COCO subsets.** We remarkably outperform three COCO pre-trained object detectors and FamNet.

Method	Val-COCO Set		Test-COCO Set	
	MAE ↓	RMSE ↓	MAE ↓	RMSE ↓
Faster RCNN [30]	52.79	172.46	36.20	79.59
RetinaNet [21]	63.57	174.36	52.67	85.86
Mask RCNN [10]	52.51	172.21	35.56	80.00
FamNet [28]	39.82	108.13	22.76	45.92
Ours	22.85	63.33	13.13	23.68

512×512 , 128×128 , and 3×3 , respectively. The number of iterations is set as 4. The model is trained with Adam optimizer [14] for 200 epochs with batch size 4 on 4 Tesla V100 GPUs. The hyper-parameter ϵ in Adam optimizer is set as $4e-11$, much smaller than the default $1e-8$, considering the small scale of the gradient. The learning rate is set as $2e-5$ initially, and it is dropped by 0.25 every 80 epochs.

Quantitative results are given in Table 1. Our approach is compared with baselines employed in [28]: FR few-shot detector [13], FSOD few-shot detector [7], Pre-trained GMN [25], GMN [25], MAML [8], FamNet [28]. Our approach outperforms all counterparts with a quite large margin. For example, our method surpasses the SOTA few-shot detector method FSOD by 21.08 MAE and 67.80 RMSE on the validation set, 18.21 MAE and 55.11 RMSE on the test set. We also excel the SOTA FSC method FamNet by 8.47 MAE and 21.87 RMSE on the validation set, 7.76 MAE and 14.00 RMSE on the test set. These significant advantages demonstrate the effectiveness of our method.

Quantitative results on COCO subsets [22, 28] are provided in Table 2. Our approach is compared with COCO pre-trained object detection methods: Faster RCNN [30], RetinaNet [21], Mask RCNN [10], and FSC approach FamNet [28]. Note that these detection networks are pre-trained on the COCO dataset containing thousands of exemplars, while our approach needs only 3 exemplars. Our approach

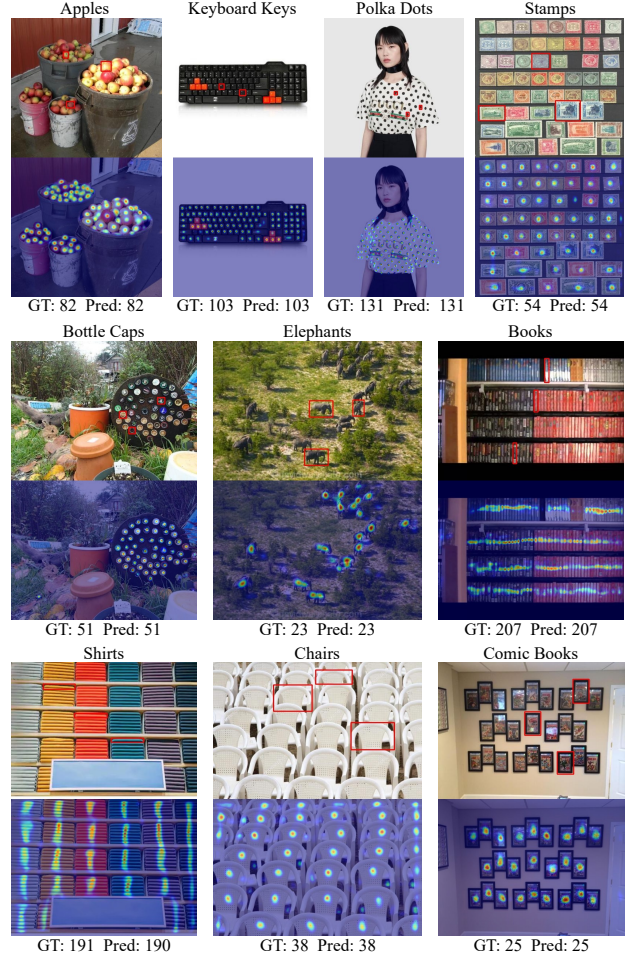


Figure 4. **Few-shot counting results on FSC-147.** From top to down: images and the predicted density maps. The objects marked by the red rectangles are the exemplars.

still surpasses Mask RCNN with a quite large margin (29.66 MAE and 108.88 RMSE on the validation set, 22.43 MAE and 56.32 RMSE on the test set). Moreover, our method significantly outperforms FSC method FamNet by 16.97 MAE and 44.80 RMSE on the validation set, 9.63 MAE and 22.24 RMSE on the test set.

Qualitative results are shown in Fig. 4. For both round objects (*e.g.* Polka Dots) and square objects (*e.g.* Stamps, Comic Books), both vertical strip objects (*e.g.* Books) and horizontal strip objects (*e.g.* Shirts), both small objects (*e.g.* Keyboard Keys) and large objects (*e.g.* Chairs), both gathered objects (*e.g.* Apples) and scattered objects (*e.g.* Elephants), our approach counts objects exactly with only a few exemplars. In particular, for Bottle Caps where the background is quite complex with lots of disturbance, our method still successfully counts target objects exactly. This verifies that our method can gradually refine the exemplar-related features and suppress exemplar-unrelated features.

Table 3. **The car counting performance on CARPK and PUCPR+.** Though designed for general class-agnostic few-shot counting, our method still surpasses all baselines.

Method	CARPK [12]		PUCPR+ [5, 12]	
	MAE ↓	RMSE ↓	MAE ↓	RMSE ↓
YOLO [29]	48.89	57.55	156.00	200.42
Faster RCNN [30]	47.45	57.39	111.40	149.35
Small RPN [12, 30]	24.32	37.62	39.88	47.67
RetinaNet [21]	16.62	22.30	24.58	33.12
LPN [12]	23.80	36.79	22.76	34.46
One Look [26]	59.46	66.84	21.88	36.73
IEP Counting [37]	51.83	-	15.17	-
GMN [25]	7.48	9.90	-	-
PDEM [9]	6.77	8.52	7.16	12.00
FamNet [28]	18.19	33.66	14.68 [†]	19.38 [†]
Ours	5.33	7.04	2.42	3.55

[†] Trained and evaluated by ourselves with the official code.

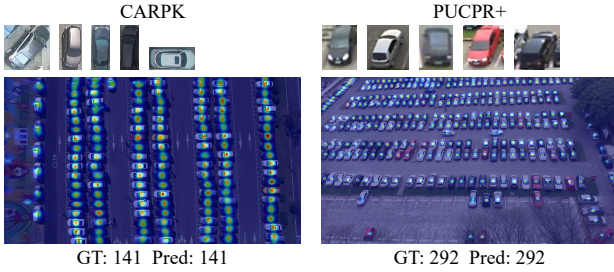


Figure 5. **Car counting results on CARPK and PUCPR+.** From top to down: the exemplars and the predicted density maps.

4.4. Class-specific Counting

Our approach is designed to be a general class-agnostic FSC approach, counting objects of novel classes with only a few exemplars. Nonetheless, we also evaluate our method on class-specific counting tasks to further testify its superiority. The setup is detailed in the Supplementary Material.

Car counting tasks are conducted on CARPK [12] and PUCPR+ [5, 12]. The quantitative results are shown in Table 3. We sample 5 exemplars from the training set. Note that these exemplars are **fixed for both training and test**. Our method is compared with *classical object detectors*: YOLO [29], Faster RCNN [30], Small RPN [12, 30], RetinaNet [21], *car counting methods*: LPN [12], One Look [26], and *general counting approaches*: IEP Counting [37], GMN [25], PDEM [9], FamNet [28]. Our approach surpasses all the compared methods considerably. Specifically, our approach surpasses PDEM by 1.44 MAE and 1.48 RMSE on CARPK, and outperforms PDEM by 4.74 MAE and 8.45 RMSE on PUCPR+. The qualitative results are shown in Fig. 5, demonstrating that our method has the ability to accurately localize and count cars.

Table 4. **The crowd counting performance (MAE ↓) on UCSD, Mall, and PartA and PartB of ShanghaiTech.** Our method surpasses all general counting methods, and achieves competitive performance on par with specific crowd counting methods.

Type	Method	UCSD [3]	Mall [4]	PartA [53]	PartB [53]
Crowd Counting	Crowd CNN [50]	1.60	-	181.8	32.0
	MCNN [53]	1.07	-	110.2	26.4
	Switch-CNN [2]	1.62	-	90.4	21.6
	CP-CNN [35]	-	-	73.6	20.1
	CNN-boost [40]	1.10	2.01	-	-
	MoC-CNN [16]	-	2.75	-	-
	CRSNet [20]	1.16	-	68.2	10.6
	RPNNet [49]	-	-	61.2	8.1
	GLF [41]	-	-	61.3	7.3
General Counting	GMN [25]	-	-	95.8	-
	LC-FCN8 [17]	1.51	2.42	-	13.14
	LC-PSPNet [17]	1.01	2.00	-	21.61
	FamNet [28]	2.70 [†]	2.64 [†]	159.11 [†]	24.90 [†]
	Ours	0.98	1.69	73.70	9.98

[†] Trained and evaluated by ourselves with the official code.

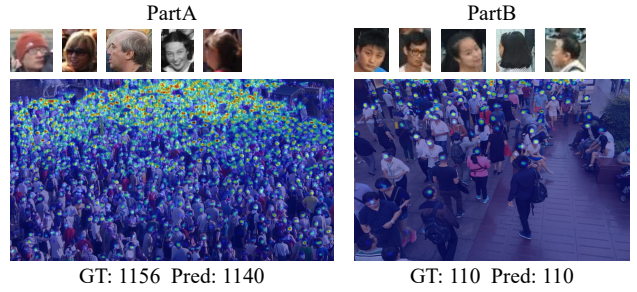


Figure 6. **Crowd counting results on ShanghaiTech.** From top to down: the exemplars and the predicted density maps.

Crowd counting tasks are implemented on UCSD [3], Mall [4], and ShanghaiTech [53], and the results of MAE are reported in Table 4. 5 exemplars are sampled from the training set and **fixed for both training and test**. The competitors include *crowd counting methods*: Crowd CNN [50], MCNN [53], Switch-CNN [2], CP-CNN [35], CNN-boost [40], MoC-CNN [16], CRSNet [20], RPNNet [49], GLF [41], and *general counting methods*: GMN [25], LC-FCN8 [17], LC-PSPNet [17], FamNet [28]. For UCSD and Mall where the crowd is relatively sparse, our approach surpasses all counterpart methods stably. For ShanghaiTech, our approach outperforms all general counting methods with a large margin, and achieves competitive performance on par with specific crowd counting methods. It is emphasized that, our method is not tailored to the specific crowd counting task, while the compared methods are. As shown in Fig. 6, our method is able to precisely localize and count crowd in extremely high-density crowd scene.

Table 5. Ablation study regarding architecture on FSC-147.

Architecture	Val Set		Test Set	
	MAE ↓	RMSE ↓	MAE ↓	RMSE ↓
Transformer	20.45	55.22	20.21	93.47
Raw Correlation	24.36	74.61	23.65	108.77
Raw Correlation + CRF	22.50	65.35	20.40	107.81
4-iter Correlation	19.74	64.30	18.70	99.34
1-iter Feature	16.23	55.34	16.46	92.62
2-iter Feature	16.04	54.53	15.36	87.35
3-iter Feature	15.78	53.39	14.74	88.22
4-iter Feature	15.28	47.20	14.32	85.54

4.5. Ablation Study

Extensive ablation studies are conducted on FSC-147 [28] to illustrate the effectiveness of the model architecture, correlation normalization, and flip operation.

Ablation study regarding architecture is conducted and the results are shown in Table 5. (a) Transformer is a 2-encoder, 2-decoder network revised based on [39], in which the exemplar features serve as k , v and the image features serve as q . q , k , v are all split into tokens. The density map is predicted using the decoder outputs. (b) Raw Correlation is similar to FamNet [28] without the test-time adaptation, predicting the density map directly from the raw correlation. (c) Raw Correlation + CRF is used to compare our refinement method with DenseCRF [15], which is a classical refinement method widely used in semantic segmentation. The raw correlation is firstly refined by DenseCRF. Then the refined correlation and the original correlation are concatenated to serve as the inputs for the density map regression. (d) The rest five methods follow our designed architecture, where i -iter Correlation and i -iter Feature mean the density maps are predicted using the correlation and the refined feature map of the i^{th} iteration, respectively.

Several conclusions could be drawn from Table 5. First, by comparing Raw Correlation with 1-iter Feature and 4-iter Correlation with 4-iter Feature, it is obvious that predicting density map from features is significantly better than predicting from correlation, because features contain much richer semantic information than correlation. Second, the performance is stably improved with the increase of the iteration number, suggesting that the exemplar-related features are gradually refined during the iterations. Third, 4-iter Feature obviously surpasses 4-layer Transformer, indicating that keeping spatial information brings substantial improvement. Fourth, our refinement modules (i -iter Feature) significantly surpass Raw Correlation + CRF. The reason can be illustrated by Fig. 7, showing that our approach is more sensitive to independent objects, while DenseCRF cannot distinguish independent objects in the gathered scene though it can derive quite clear region boundaries.

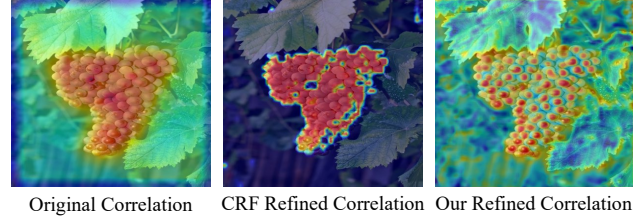


Figure 7. Comparison between our refinement approach and DenseCRF refinement. Our refinement approach is much more sensitive to independent objects.

Table 6. Ablation study regarding correlation normalization and flip operation on FSC-147.

			Val Set		Test Set	
EN	SN	Flip	MAE ↓	RMSE ↓	MAE ↓	RMSE ↓
✗	✗	✓	22.19	66.52	20.48	99.74
✓	✗	✓	16.55	51.87	15.14	85.65
✗	✓	✓	16.58	51.26	16.40	93.97
✓	✓	✗	16.78	57.47	15.35	93.59
✓	✓	✓	15.28	47.20	14.32	85.54

Ablation study regarding correlation normalization and flip operation is carried out and the results are shown in Table 6. Without correlation normalization, we still stably outperform FamNet [28], indicating the effectiveness of our architecture. Adding either exemplar normalization (EN) or spatial normalization (SN) improves the performance greatly. EN together with SN brings the best performance, indicating the significance of the proposed normalization modules. Without flip, namely, the correlated feature map is calculated by direct convolution and add operations, the performance still remarkably surpasses FamNet [28]. Adding flip further improves the performance, because the flip helps the correlated feature map maintain consistent spatial structure as the exemplar feature map.

5. Conclusion

In this paper, we propose an iterative few-shot counting framework including a Correlation Distillation module and a Feature Refinement module to gradually refine the exemplar-related features. The density map is predicted from the final refined feature map. We conduct extensive experiments on the few-shot counting benchmark FSC-147, car counting benchmarks CARPK and PUCPR+, and crowd counting benchmarks UCSD, Mall, and ShanghaiTech. Our approach achieves state-of-the-art performance on FSC-147, CARPK, PUCPR+, UCSD, and Mall. We also achieve competitive performance on ShanghaiTech, though our approach is de facto a general class-agnostic FSC method.

References

- [1] Carlos Arteta, Victor Lempitsky, and Andrew Zisserman. Counting in the wild. In *ECCV*, pages 483–498, 2016. 1, 2
- [2] Deepak Babu Sam, Shiv Surya, and R Venkatesh Babu. Switching convolutional neural network for crowd counting. In *CVPR*, pages 5744–5752, 2017. 2, 7
- [3] Antoni B Chan, Zhang-Sheng John Liang, and Nuno Vasconcelos. Privacy preserving crowd monitoring: Counting people without people models or tracking. In *CVPR*, pages 1–7, 2008. 2, 5, 7
- [4] Ke Chen, Chen Change Loy, Shaogang Gong, and Tony Xiang. Feature mining for localised crowd counting. In *BMVC*, volume 1, page 3, 2012. 2, 5, 7
- [5] Paulo RL De Almeida, Luiz S Oliveira, Alceu S Britto Jr, Eunelson J Silva Jr, and Alessandro L Koerich. PKLot—A robust dataset for parking lot classification. *Expert Systems with Applications*, 42(11):4937–4949, 2015. 1, 2, 5, 7
- [6] Qi Fan, Wei Zhuo, Chi-Keung Tang, and Yu-Wing Tai. Few-shot object detection with attention-rpn and multi-relation detector. In *CVPR*, pages 4013–4022, 2020. 3
- [7] Qi Fan, Wei Zhuo, Chi-Keung Tang, and Yu-Wing Tai. Few-shot object detection with attention-rpn and multi-relation detector. In *CVPR*, pages 4013–4022, 2020. 6
- [8] Chelsea Finn, Pieter Abbeel, and Sergey Levine. Model-agnostic meta-learning for fast adaptation of deep networks. In *ICML*, pages 1126–1135. PMLR, 2017. 3, 6
- [9] Eran Goldman, Roei Herzig, Aviv Eisenschtat, Jacob Goldberger, and Tal Hassner. Precise detection in densely packed scenes. In *CVPR*, pages 5227–5236, 2019. 2, 5, 7
- [10] Kaiming He, Georgia Gkioxari, Piotr Dollár, and Ross Girshick. Mask R-CNN. In *ICCV*, pages 2961–2969, 2017. 6
- [11] Kaiming He, Xiangyu Zhang, Shaoqing Ren, and Jian Sun. Deep residual learning for image recognition. In *CVPR*, pages 770–778, 2016. 3
- [12] Meng-Ru Hsieh, Yen-Liang Lin, and Winston H Hsu. Drone-based object counting by spatially regularized regional proposal network. In *ICCV*, pages 4145–4153, 2017. 1, 2, 5, 7
- [13] Bingyi Kang, Zhuang Liu, Xin Wang, Fisher Yu, Jiashi Feng, and Trevor Darrell. Few-shot object detection via feature reweighting. In *ICCV*, pages 8420–8429, 2019. 6
- [14] Diederik P Kingma and Jimmy Ba. Adam: A method for stochastic optimization. *arXiv preprint arXiv:1412.6980*, 2014. 6
- [15] Philipp Krähenbühl and Vladlen Koltun. Efficient inference in fully connected crfs with gaussian edge potentials. *NeurIPS*, 24:109–117, 2011. 8
- [16] Shohei Kumagai, Kazuhiro Hotta, and Takio Kurita. Mixture of counting cnns. *Machine Vision and Applications*, 29(7):1119–1126, 2018. 7
- [17] Issam H Laradji, Negar Rostamzadeh, Pedro O Pinheiro, David Vazquez, and Mark Schmidt. Where are the blobs: Counting by localization with point supervision. In *ECCV*, pages 547–562, 2018. 2, 7
- [18] Bastian Leibe, Edgar Seemann, and Bernt Schiele. Pedestrian detection in crowded scenes. In *CVPR*, volume 1, pages 878–885, 2005. 2
- [19] Victor Lempitsky and Andrew Zisserman. Learning to count objects in images. *NeurIPS*, 23:1324–1332, 2010. 2
- [20] Yuhong Li, Xiaofan Zhang, and Deming Chen. Csrnet: Dilated convolutional neural networks for understanding the highly congested scenes. In *CVPR*, pages 1091–1100, 2018. 7
- [21] Tsung-Yi Lin, Priya Goyal, Ross Girshick, Kaiming He, and Piotr Dollár. Focal loss for dense object detection. In *ICCV*, pages 2980–2988, 2017. 6, 7
- [22] Tsung-Yi Lin, Michael Maire, Serge Belongie, James Hays, Pietro Perona, Deva Ramanan, Piotr Dollár, and C Lawrence Zitnick. Microsoft COCO: Common objects in context. In *ECCV*, pages 740–755, 2014. 5, 6
- [23] Jiang Liu, Chenqiang Gao, Deyu Meng, and Alexander G Hauptmann. Decidenet: Counting varying density crowds through attention guided detection and density estimation. In *CVPR*, pages 5197–5206, 2018. 2
- [24] Lingbo Liu, Jiaqi Chen, Hefeng Wu, Guanbin Li, Chenglong Li, and Liang Lin. Cross-modal collaborative representation learning and a large-scale rgbt benchmark for crowd counting. In *CVPR*, pages 4823–4833, 2021. 1, 2, 5
- [25] Erika Lu, Weidi Xie, and Andrew Zisserman. Class-agnostic counting. In *ACCV*, pages 669–684, 2018. 1, 2, 6, 7
- [26] T Nathan Mundhenk, Goran Konjevod, Wesam A Sakla, and Kofi Boakye. A large contextual dataset for classification, detection and counting of cars with deep learning. In *ECCV*, pages 785–800, 2016. 7
- [27] Viresh Ranjan, Hieu Le, and Minh Hoai. Iterative crowd counting. In *ECCV*, pages 270–285, 2018. 2
- [28] Viresh Ranjan, Udbhav Sharma, Thu Nguyen, and Minh Hoai. Learning to count everything. In *CVPR*, pages 3394–3403, 2021. 1, 2, 3, 4, 5, 6, 7, 8
- [29] Joseph Redmon, Santosh Divvala, Ross Girshick, and Ali Farhadi. You only look once: Unified, real-time object detection. In *CVPR*, pages 779–788, 2016. 7
- [30] Shaoqing Ren, Kaiming He, Ross Girshick, and Jian Sun. Faster R-CNN: Towards real-time object detection with region proposal networks. *NeurIPS*, 28:91–99, 2015. 3, 6, 7
- [31] Olga Russakovsky, Jia Deng, Hao Su, Jonathan Krause, Sanjeev Satheesh, Sean Ma, Zhiheng Huang, Andrej Karpathy, Aditya Khosla, Michael Bernstein, et al. Imagenet large scale visual recognition challenge. *IJCV*, 115(3):211–252, 2015. 2
- [32] Deepak Babu Sam and R Venkatesh Babu. Top-down feedback for crowd counting convolutional neural network. In *AAAI*, 2018. 2
- [33] Zenglin Shi, Le Zhang, Yun Liu, Xiaofeng Cao, Yangdong Ye, Ming-Ming Cheng, and Guoyan Zheng. Crowd counting with deep negative correlation learning. In *CVPR*, pages 5382–5390, 2018. 2
- [34] Vishwanath A Sindagi and Vishal M Patel. Generating high-quality crowd density maps using contextual pyramid cnns. In *ICCV*, pages 1861–1870, 2017. 2

- [35] Vishwanath A Sindagi and Vishal M Patel. Generating high-quality crowd density maps using contextual pyramid cnns. In *ICCV*, pages 1861–1870, 2017. 7
- [36] Qingyu Song, Changan Wang, Zhengkai Jiang, Yabiao Wang, Ying Tai, Chengjie Wang, Jilin Li, Feiyue Huang, and Yang Wu. Rethinking counting and localization in crowds: A purely point-based framework. *arXiv preprint arXiv:2107.12746*, 2021. 1, 2
- [37] T. Stahl, S. L. Pinteá, and Jcv Gemert. Divide and count: Generic object counting by image divisions. *TIP*, 28(2):1035–1044, 2019. 2, 7
- [38] Russell Stewart, Mykhaylo Andriluka, and Andrew Y Ng. End-to-end people detection in crowded scenes. In *CVPR*, pages 2325–2333, 2016. 2
- [39] Ashish Vaswani, Noam Shazeer, Niki Parmar, Jakob Uszkoreit, Llion Jones, Aidan N Gomez, Łukasz Kaiser, and Illia Polosukhin. Attention is all you need. In *NeurIPS*, pages 5998–6008, 2017. 5, 8
- [40] Elad Walach and Lior Wolf. Learning to count with cnn boosting. In *ECCV*, pages 660–676, 2016. 7
- [41] Jia Wan, Ziquan Liu, and Antoni B Chan. A generalized loss function for crowd counting and localization. In *CVPR*, pages 1974–1983, 2021. 2, 7
- [42] Jia Wan, Wenhan Luo, Baoyuan Wu, Antoni B Chan, and Wei Liu. Residual regression with semantic prior for crowd counting. In *CVPR*, pages 4036–4045, 2019. 2
- [43] Meng Wang and Xiaogang Wang. Automatic adaptation of a generic pedestrian detector to a specific traffic scene. In *CVPR*, pages 3401–3408, 2011. 2
- [44] Davis Wertheimer, Luming Tang, and Bharath Hariharan. Few-shot classification with feature map reconstruction networks. In *CVPR*, pages 8012–8021, 2021. 3
- [45] Jiaxi Wu, Songtao Liu, Di Huang, and Yunhong Wang. Multi-scale positive sample refinement for few-shot object detection. In *ECCV*, pages 456–472, 2020. 3
- [46] Feng Xiong, Xingjian Shi, and Dit-Yan Yeung. Spatiotemporal modeling for crowd counting in videos. In *ICCV*, pages 5151–5159, 2017. 2
- [47] Zhaoyi Yan, Yuchen Yuan, Wangmeng Zuo, Xiao Tan, Yezhen Wang, Shilei Wen, and Errui Ding. Perspective-guided convolution networks for crowd counting. In *ICCV*, pages 952–961, 2019. 2
- [48] Lihe Yang, Wei Zhuo, Lei Qi, Yinghuan Shi, and Yang Gao. Mining latent classes for few-shot segmentation. *arXiv preprint arXiv:2103.15402*, 2021. 3
- [49] Yifan Yang, Guorong Li, Zhe Wu, Li Su, Qingming Huang, and Nicu Sebe. Reverse perspective network for perspective-aware object counting. In *CVPR*, pages 4374–4383, 2020. 2, 7
- [50] Cong Zhang, Hongsheng Li, Xiaogang Wang, and Xiaokang Yang. Cross-scene crowd counting via deep convolutional neural networks. In *CVPR*, pages 833–841, 2015. 2, 7
- [51] Chi Zhang, Guosheng Lin, Fayao Liu, Rui Yao, and Chunhua Shen. Canet: Class-agnostic segmentation networks with iterative refinement and attentive few-shot learning. In *CVPR*, pages 5217–5226, 2019. 3
- [52] Qi Zhang, Wei Lin, and Antoni B Chan. Cross-view cross-scene multi-view crowd counting. In *CVPR*, pages 557–567, 2021. 1, 2
- [53] Yingying Zhang, Desen Zhou, Siqin Chen, Shenghua Gao, and Yi Ma. Single-image crowd counting via multi-column convolutional neural network. In *CVPR*, pages 589–597, 2016. 1, 2, 5, 7